

Fréedericksz transition under electric and rotating magnetic field: application to nematics with negative dielectric and magnetic anisotropies

P. Oswald, G. Poy & F. Vittoz

To cite this article: P. Oswald, G. Poy & F. Vittoz (2017): Fréedericksz transition under electric and rotating magnetic field: application to nematics with negative dielectric and magnetic anisotropies, *Liquid Crystals*, DOI: [10.1080/02678292.2016.1272722](https://doi.org/10.1080/02678292.2016.1272722)

To link to this article: <http://dx.doi.org/10.1080/02678292.2016.1272722>



Published online: 02 Feb 2017.



Submit your article to this journal [↗](#)



Article views: 46



View related articles [↗](#)



View Crossmark data [↗](#)

Fréedericksz transition under electric and rotating magnetic field: application to nematics with negative dielectric and magnetic anisotropies

P. Oswald, G. Poy and F. Vittoz

Laboratoire de Physique, Univ Lyon, ENS de Lyon, Univ Claude Bernard, CNRS, Lyon, France

ABSTRACT

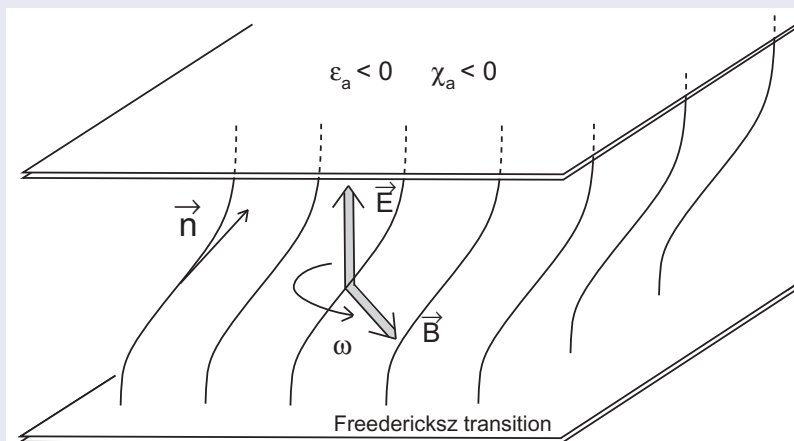
We study the action of a rotating magnetic field on the Fréedericksz instability under electric field of a homeotropic nematic sample sandwiched between two parallel electrodes. The liquid crystal (LC) is of negative dielectric and magnetic anisotropies and the magnetic field is parallel to the electrodes used to apply the electric field. We show that the sample destabilises above a critical voltage V_c that depends on the magnetic field B and its angular rotation velocity ω . The relation $V_c(B, \omega)$ is calculated analytically in the synchronous regime, where the director rotates at the same angular velocity as the magnetic field. These predictions are compared to the experiment performed with the LC CCN-37. From this experiment, the values of the bend constant K_3 , of the rotational viscosity γ_1 and of the magnetic anisotropy χ_a are deduced.

ARTICLE HISTORY

Received 3 November 2016
Accepted 12 December 2016

KEYWORDS



Nematic liquid crystals;
Fréedericksz transition;
rotating magnetic field;
magnetic anisotropy




1. Introduction

The Fréedericksz transition [1] is a bifurcation between two nematic states: a uniform state in which the director is oriented in a single direction and a distorted state in which the director field is distorted upon application of a strong enough magnetic or electric field. This transition is important in practice because the fabrication of the liquid crystal (LC) displays [2,3] used in our daily life is based on it. This transition is also very useful for measuring the three elastic constants K_i ($i = 1 - 3$) of the nematic phase. The most usual technique described in all textbooks on LC consists of submitting a planar (or homeotropic) nematic sample to a magnetic (or electric) field parallel or perpendicular to the plates

limiting the sample. Measuring the critical electric (or magnetic) field yields the ratios K_i/ϵ_a (or K_i/χ_a), where K_i depends on the geometry chosen [4]. The elastic constant can then be calculated, provided the dielectric (or magnetic) anisotropy ϵ_a (or χ_a) is known. In practice, the dielectric constants – and consequently their anisotropy – are easy to measure with a LCR meter. By contrast, the magnetic anisotropy is more difficult to measure because the materials are diamagnetic (with very small magnetic susceptibilities). In practice, several methods have been used to measure χ_a . Some of them, as the Faraday–Curie method [5,6], the Gouy balance method [7] or those using a superconducting quantum interference device [8], are indirect and consist in

CONTACT P. Oswald  patrick.oswald@ens-lyon.fr  Laboratoire de Physique, Univ Lyon, ENS de Lyon, Univ Claude Bernard, CNRS, F-69342 Lyon, France

 Supplemental data for this article can be accessed [here](#).

© 2017 Informa UK Limited, trading as Taylor & Francis Group

measuring χ_{\parallel} (if $\chi_a > 0$) or χ_{\perp} (if $\chi_a < 0$) in a bulk nematic sample and $\bar{\chi} = (\chi_{\parallel} + 2\chi_{\perp})/3$ – a quantity which does not depend on temperature because the material is diamagnetic – in the isotropic liquid. From these two measurements, χ_a can be deduced. In another technique, a bulk nematic sample is subjected to a rotating magnetic field B . Measuring the maximum torque that the field exerts on the sample directly gives the magnetic anisotropy. But this method works only with materials of positive magnetic anisotropy [9]. Another method, simpler to implement, is to impose a strong magnetic field that stabilises the initial director configuration in an oriented sample. Measuring the increase of the critical voltage necessary to destabilise the structure gives the ratio χ_a/ϵ_a from which χ_a can be deduced knowing ϵ_a . This method was successfully applied by Schad et al. [10] to materials with positive or negative χ_a , but positive ϵ_a . On the other hand, this method is not easily applicable to the materials with negative dielectric and magnetic anisotropies which are considered in this article. Indeed, the only possibility would be to use a homeotropic sample with the two fields perpendicular to the plates or a planar sample with the two fields parallel to the anchoring direction. In these two configurations, the two fields are destabilising. The ratio χ_a/ϵ_a could be obtained by measuring the decrease of the critical electric field when the magnetic field is smaller than the critical magnetic field necessary to destabilise the structure at zero electric field. The difficulty here is to impose, either a magnetic field perpendicular to the sample (we do not have the appropriate electromagnet) or an electric field parallel to the sample.

For this reason, we looked for another technique using a Halbach array. With this permanent magnet, a very homogeneous magnetic field B can be applied in the plane of the sample. In this article, we show theoretically and experimentally that the onset of instability under electric field of a homeotropic sample increases when it is submitted to a

magnetic field parallel to the plates and rotating at angular velocity ω . By measuring the critical voltage $V_c(\omega)$ as a function of ω , or equivalently, the critical rotation velocity $\omega_c(V)$ above which the sample restabilises when it is subjected to a voltage V larger than V_F (the Fréedericksz critical voltage at $B = 0$), we show that it is possible to measure the ratios K_3/ϵ_a , ϵ_a/χ_a and γ_1/χ_a , where γ_1 is the rotational viscosity. This technique is applied to the LC CCN-37 which has dielectric and magnetic anisotropies both negative [11].

2. Theoretical analysis

We consider a nematic sample sandwiched between two parallel electrodes at $z = 0$ and $z = d$ treated for strong homeotropic anchoring. The director orientation is given by the zenith angle θ and the azimuthal angle φ . The electric field \vec{E} is parallel to the z -axis and the magnetic field \vec{B} is parallel to the xy -plane and rotates with the angular velocity ω (Figure 1). For simplicity, we present here the calculation in isotropic elasticity ($K = K_1 = K_2 = K_3$) by further assuming that the electric field is constant: $E = V/d$, where V is the applied voltage. The complete calculation in anisotropic elasticity and taking into account the electric field variation within the nematic layer is given in the Appendix. By neglecting the backflow effect (this approximation is justified experimentally, see section 4), the torque equations read

$$\begin{aligned} \gamma_1 \frac{\partial \theta}{\partial t} = & K \frac{\partial^2 \theta}{\partial z^2} - K \sin \theta \cos \theta \left(\frac{\partial \varphi}{\partial z} \right)^2 \\ & - \epsilon_0 \epsilon_a E^2 \sin \theta \cos \theta \\ & + \frac{\chi_a B^2}{\mu_0} \sin \theta \cos \theta \cos^2(\varphi - \omega t), \end{aligned} \quad (1)$$

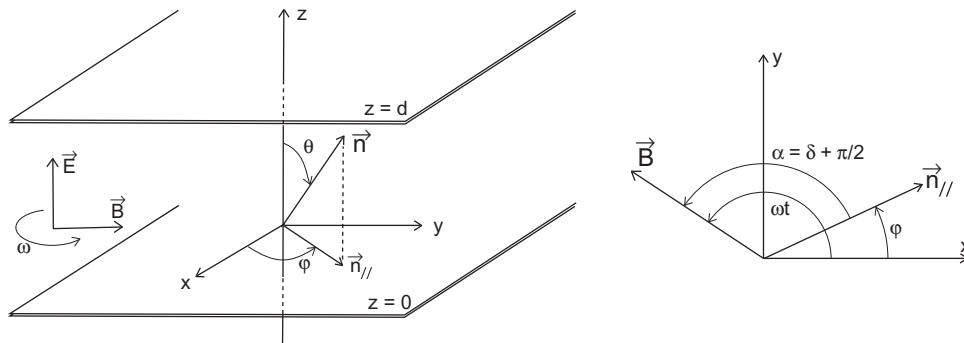


Figure 1. Definition of angles θ and φ and of the phase lag α .

$$\gamma_1 \frac{\partial \varphi}{\partial t} = K \frac{\partial^2 \varphi}{\partial z^2} + K \cot \theta \left(\frac{\partial \varphi}{\partial z} \right) \left(\frac{\partial \theta}{\partial z} \right) - \frac{\chi_a B^2}{\mu_0} \sin(\varphi - \omega t) \cos(\varphi - \omega t), \quad (2)$$

where ϵ_0 is the vacuum permittivity. We look for a stationary solution of the form $\varphi(t) = \omega t - \alpha$ with α a constant and $\theta(z)$ only function of z . After substitution into Equation (2), one obtains the phase lag $\alpha = \pi/2 + \delta$ between the magnetic field and the projection of the director onto the xy -plane (Figure 1) with

$$\delta = \frac{1}{2} \arcsin \left(\frac{\omega}{\omega_*} \right), \quad (3)$$

and

$$\omega_* = \frac{-\chi_a B^2}{2\gamma_1 \mu_0}. \quad (4)$$

Equation (3) shows that this solution exists only when $\omega < \omega_*$. This defines the limit between the synchronous regime and the asynchronous regime [9,12]. In the following, we restrict our analysis to the synchronous regime ($\omega \leq \omega_*$). Another important point is that α does not depend on the applied voltage, providing that the voltage is larger than V_F .

The angle $\theta(z)$ is obtained by replacing φ by its expression into Equation (2). This gives

$$\frac{d^2 \theta}{dz^2} = - \left[\frac{1}{\xi_e^2} - \frac{1 - \sqrt{1 - \left(\frac{\omega}{\omega_*} \right)^2}}{2\xi_m^2} \right] \sin \theta \cos \theta, \quad (5)$$

where ξ_e and ξ_m are the electric and magnetic coherence lengths, respectively [4]:

$$\xi_e^2 = \frac{-K}{\epsilon_0 \epsilon_a E^2} \quad \text{and} \quad \xi_m^2 = \frac{-\mu_0 K}{\chi_a B^2}. \quad (6)$$

By setting $Z = \pi z/d$, this equation can be rewritten in the form

$$\frac{d^2 \theta}{dZ^2} = - \left(\frac{V^2 - V_B^2}{V_F^2} \right) \sin \theta \cos \theta, \quad (7)$$

where $V_F = \pi \sqrt{\frac{K}{-\epsilon_0 \epsilon_a}}$ is the usual critical voltage at zero magnetic field (or under a static magnetic field in this experiment) and

$$V_B^2 = V_0^2 \left[1 - \sqrt{1 - \left(\frac{\omega}{\omega_*} \right)^2} \right] \quad \text{with} \quad V_0 = \sqrt{\frac{\chi_a}{2\epsilon_a}} B d c \quad (8)$$

and c the velocity of light. Integrating Equation (5) gives

$$Z \sqrt{\frac{V^2 - V_B^2}{V_F^2}} = \int_0^{\theta(Z)} \frac{d\theta'}{\sqrt{\sin^2 \theta_m - \sin^2 \theta'}} = \int_0^{\arcsin \left(\frac{\sin \theta(Z)}{\sin \theta_m} \right)} \frac{d\psi}{\sqrt{1 - \sin^2 \theta_m \sin^2 \psi}}, \quad (9)$$

where θ_m denotes the maximum tilt angle in the middle of the cell (at $Z = \pi/2$) and $\sin \theta' = \sin \theta_m \sin \psi$. From this equation, the profile $\theta(Z)$ can be calculated numerically. More important, this equation shows that at $Z = \pi/2$, the angle θ_m satisfies the equation

$$\frac{\pi}{2} \sqrt{\frac{V^2 - V_B^2}{V_F^2}} = \int_0^{\pi/2} \frac{d\psi}{\sqrt{1 - \sin^2 \theta_m \sin^2 \psi}} = K(\sin \theta_m), \quad (10)$$

where $K(x)$ is the complete elliptic integral of the first kind. Because $K(x) > \frac{\pi}{2} \forall x$, we deduce that the homeotropic sample destabilises when $\frac{V^2 - V_B^2}{V_F^2} \geq 1$. This defines the onset of instability $V_c(\omega)$ which depends on the angular velocity of the magnetic field:

$$\begin{aligned} \frac{V_c(\omega)}{V_F} &= \sqrt{1 + \frac{V_B^2}{V_F^2}} \\ &= \sqrt{1 + \frac{V_0^2}{V_F^2} \left[1 - \sqrt{1 - \left(\frac{\omega}{\omega_*} \right)^2} \right]} \end{aligned} \quad (11)$$

where $V_0^2 \propto B^2$ is given in Equation (8), or equivalently, the critical velocity $\omega_c(V)$ above which the sample restabilises when it is submitted to a voltage $V \geq V_F$:

$$\frac{\omega_c(V)}{\omega_*} = \sqrt{1 - \left(1 - \frac{V^2 - V_F^2}{V_0^2} \right)^2} \quad (12)$$

Note that these equations are only valid in the synchronous regime to which we restrict our analysis. A schematic phase diagram is shown in Figure 2. In the Appendix, we show that this equation remains unchanged in the general case on condition to take $K = K_3$.

This analysis shows that the onset of the Fréedericksz transition in the bend geometry (homeotropic sample) increases under the action of a rotating magnetic field in the synchronous regime. This effect is original because the onset remains unchanged when the field is static, which is not the case in the usual experiments performed under crossed fields as in [10].

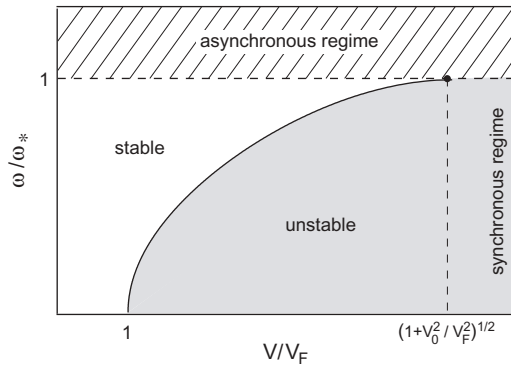


Figure 2. Phase diagram in the plane of the parameters ω/ω_* and V/V_F . Only the synchronous regime was considered.

From the measurement of $V_c(\omega)$ (or equivalently $\omega_c(V)$ when $V > V_F$), the ratios K_3/ϵ_a and ϵ_a/χ_a can be deduced. In addition, the measurement of the phase lag $\alpha(\omega)$ gives the ratio γ_1/χ_a according to Equations (3) and (4). In the following, we apply these results to the measurement of K_3 , χ_a and γ_1 in the LC CCN-37.

3. Material and experimental set-up

The LC chosen is CCN-37 (or $4\alpha,4'\alpha$ -propylheptyl-1 $\alpha,1'\alpha$ -bicyclohexyl-4 β -carbonitrile from Nematel GmbH & Co. KG, Mainz, Germany). This LC has a nematic phase between 22.5°C and 54.1°C [11]. Its dielectric anisotropy – that we and Merck have previously measured [11,14], is negative and well fitted by formula $\epsilon_a = -7.0963 + 0.06534\delta T + 3.8563/(0.26291 - \delta T)^{0.17576}$, where $\delta T = T - T_{NI}$ is given in kelvin (where T_{NI} is the nematic-isotropic transition temperature). The sample is prepared between two parallel indium tin oxide electrodes treated for homeotropic anchoring with the Nissan polyimide 0626. Nylon wires are used as a spacer and the sample thickness is measured to within $\pm 0.1 \mu\text{m}$ with a spectrometer. The sample is placed in an oven regulated to within $\pm 0.02^\circ\text{C}$, thanks to an ATNE controller. The rotating magnetic field is imposed by placing the oven and the sample inside a Halbach magnet which can rotate about its revolution axis and produces a horizontal 1 T magnetic field in its centre. The experimental set-up, already described in detail in [15] and [13], was modified by one of us (F.V.) in order that the magnet and its drive motor are mechanically decoupled from the oven and the microscope used to observe the sample. In this way, no vibration is now transmitted from the motor to the sample. A schematic representation of our set-up is shown in Figure 3 where two photodiodes are visible. The first one PD1 gives a signal I_1 of frequency 2ω , the phase of which Φ_1 gives the orientation of the magnetic field. The other PD2 gives a signal I_2 of

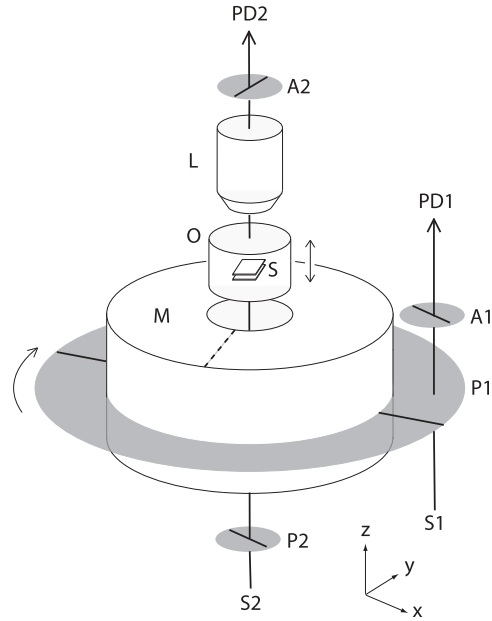


Figure 3. Schematic representation of the experimental set-up (from [13], M is the magnet (Halbach array), O is the oven which can be moved along the vertical axis and S is the sample. L is a microscope objective with a long working distance. PD1 and PD2 are two photodiodes. S1 is a red LED source and S2 is a white light source. P1 is a rotating polariser attached to the magnet, P2 is a fixed polariser and A1 and A2 are two fixed analysers. The dashed line drawn on the upper side of the magnet indicates the direction of the magnetic field along the revolution axis of the magnet. Note that in this experiment, the oven is placed in the centre of the magnet where the magnetic field is the strongest ($B = 1 \text{ T}$) and the most homogeneous.

frequency 4ω , the phase of which Φ_2 directly gives the orientation of the director projector \vec{n}_{\parallel} in the horizontal plane (knowing that the director remains everywhere in the same vertical plane in the synchronous regime). Finally, the sample can be directly observed through the microscope which is useful to check the quality of the homeotropic anchoring. A three-dimensional PDF view of the complete set-up is shown in the supplemental material.

4. Experimental results

All experiments were performed with a sample of thickness $d = 70.5 \mu\text{m}$ and an alternating current voltage of frequency 1 kHz. We first measured the critical voltage V_F above which the sample destabilises when the magnet does not rotate. In this case, the only action of the magnetic field is to lift the degeneracy about the tilt direction of the director in the sample thickness above V_F . The measurements were performed by directly observing the sample between crossed polarisers at 45° to the magnetic field, while simultaneously

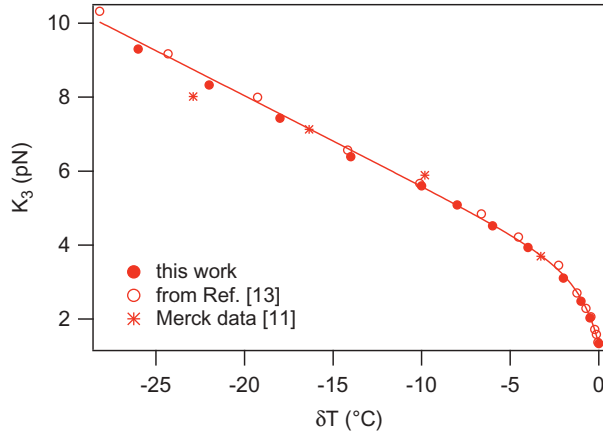


Figure 4. (colour online) Bend elastic constant K_3 as a function of temperature and its fit (solid line) with the formula given in the text.

measuring the cell capacitance with a HP 4284A LCR meter. Both methods gave the same results. From these measurements, K_3 was obtained by using the formula for ε_a given earlier. These measurements are in good agreement with previous ones performed in a much thinner sample (see [14]) and with Merck data [11]. All of our data (including those of [14]) are well fitted with formula

$$K_3(\text{pN}) = 3.18 - 0.243 \delta T - 79.4/(3.5 - \delta T)^3$$

as can be seen in Figure 4. We then measured the phase lag α (or equivalently $\delta = \alpha - \pi/2$) as a function of the rotation velocity ω by using the same procedure as in [13,15]. First, we checked that at each temperature the curves $\delta(\omega)$ obtained for different values of $V > V_F$ were superposable (Figure 5), in agreement with our model (see Equation (3)). This shows that the backflow effect is negligible in this experiment (at least when optical measurements are done in the middle of the sample) and that the measured rotational

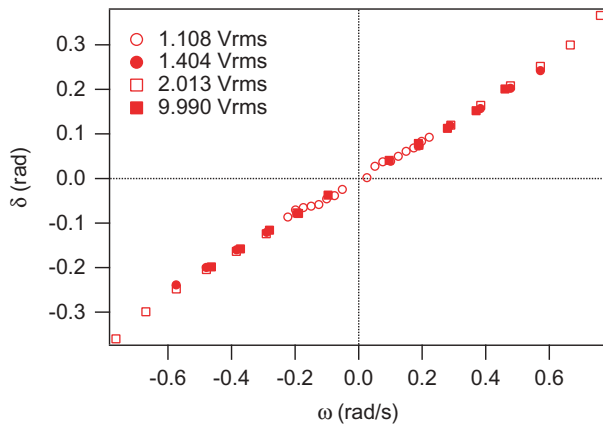


Figure 5. (colour online) Phase lag $\delta = \alpha - \pi/2$ as a function of the rotation velocity ω measured for different values of the applied voltage. $\delta T = -4^\circ\text{C}$ and $V_F = 0.99 V_{\text{rms}}$.

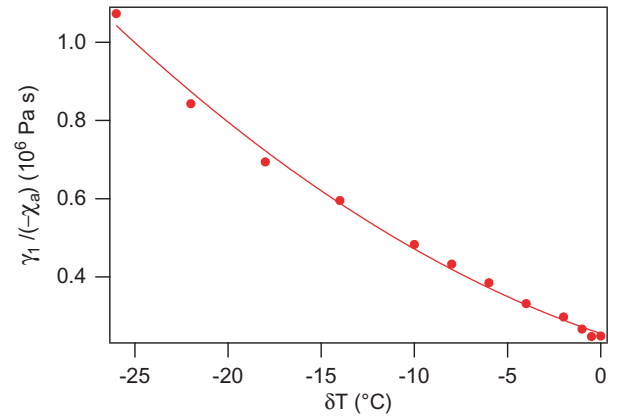


Figure 6. (colour online) Ratio $\gamma_1/(-\chi_a)$ as a function of temperature. The solid line is just a guide for the eye.

viscosity is very close to γ_1 . The same conclusion was already reached in our previous experiments conducted with nematic LCs of positive magnetic anisotropy [13]. Second, we systematically measured the slope at the origin m of the curve $\delta(\omega)$ as a function temperature. From this measurement, the ratio $\gamma_1/(-\chi_a)$ was calculated knowing that $\gamma_1/(-\chi_a) = mB^2/\mu_0$, according to Equations (3) and (4) (Figure 6). Finally, we measured the critical velocity ω_c above which the instability disappears when a voltage $V > V_F$ is applied. This was done by measuring the average value of the transmitted intensity through the sample between crossed polarisers as a function of ω . Typical curves are shown in Figure 7. They show that the mean intensity decreases linearly with the rotation velocity and vanishes above a critical velocity ω_c , meaning that the sample is again homeotropic. It can be noted that the transition is continuous, as predicted by the theory, but slightly smoothed near ω_c . This could be due to the fact that the magnetic field is certainly not exactly parallel to the

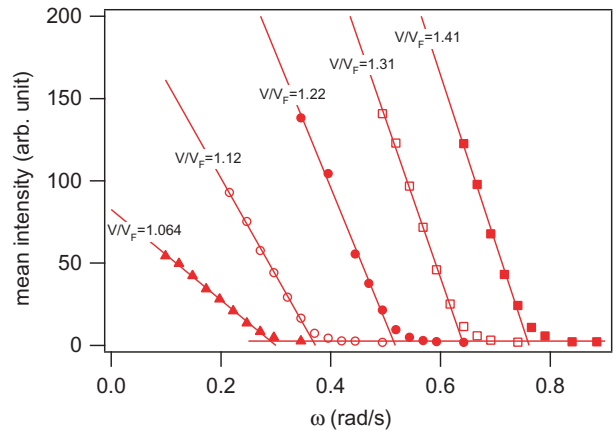


Figure 7. (colour online) Mean intensity between crossed polarisers as a function of the rotation velocity ω . Each curve was measured for a different value of the ratio V/V_F . $\delta T = -4^\circ\text{C}$.

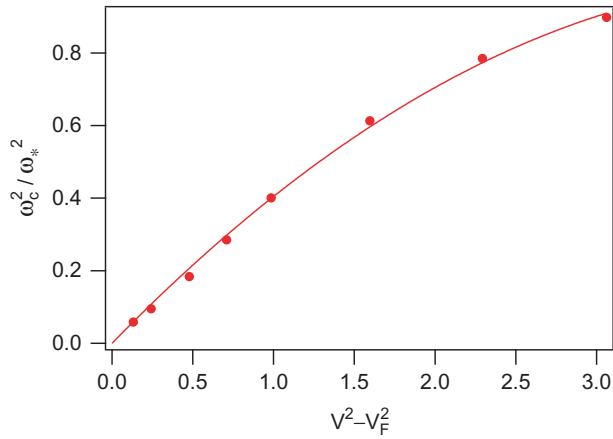


Figure 8. (colour online) Ratio ω_c^2/ω_*^2 as a function of the difference $V^2 - V_F^2$. The solid line is the best fit to Equation (12) with $V_0 = 2.09V_{rms}$.

plane of the sample. Finally, a typical curve ω_c^2/ω_*^2 (with $\omega_* = 1/(2m)$) as a function of $V^2 - V_F^2$ is shown in Figure 8 together with its best fit to Equation (12) where the only adjustable parameter is V_0 . Again the agreement between theory and experiment is good. From this fit, V_0 and, thus, the ratio χ_a/ϵ_a can be obtained by using Equation (8). The magnetic anisotropy χ_a was then calculated since ϵ_a is known. The same procedure was repeated at other temperatures to obtain the curve $\chi_a(\delta T)$ shown in Figure 9. Finally, the rotational viscosity γ_1 was calculated from the data in Figure 6 by using our values of χ_a . The result is shown in Figure 10. It must be noted here that our values of χ_a are rather different from those given by Merck [11] as can be seen in Figure 9. The origin of this disagreement is unknown. On the other hand, the value of γ_1 that we find at the transition, $\gamma_1(T_{NI}) = 0.0079$ Pa s, agrees well with the value previously measured by using the Fréedericksz

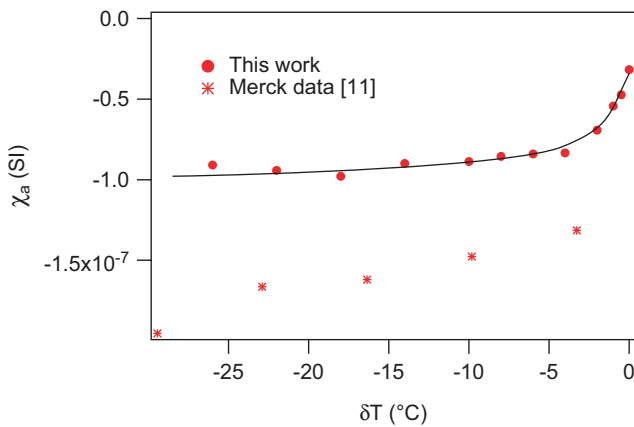


Figure 9. (colour online) Magnetic anisotropy χ_a as a function of temperature. The solid line is just a guide for the eye.

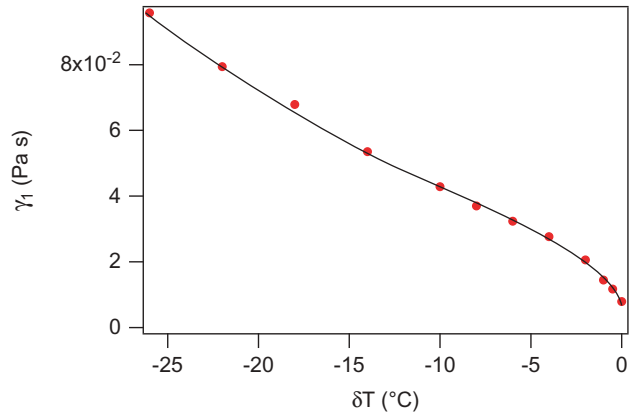


Figure 10. (colour online) Rotational viscosity γ_1 as a function of temperature. The solid line is just a guide for the eye.

transition in the bend geometry after correction of the backflow effect: $\gamma_1(T_{NI}) = 0.0074$ Pa [14]. This agreement confirms that our value of the magnetic anisotropy at the transition is actually correct.

5. Conclusion

We have shown that a rotating magnetic field parallel to the electrodes increases the Fréedericksz critical voltage in the bend geometry when the LC is of negative dielectric and magnetic anisotropies. This phenomenon can be used to measure the ratio ϵ_a/χ_a and generalises the classical method of the Fréedericksz transition under crossed fields used so far to measure this ratio when one of the fields (usually the magnetic one) is stabilising while the other (usually the electric one) is destabilising. The originality here is that the magnetic field is ‘neutral’ at rest and becomes only stabilising when it is rotating. In our study, the calculations – and the measurements with the LC CCN-37 – were performed in the synchronous regime in which the director rotates at the same velocity as the magnetic field. Nevertheless, this phenomenon should also exist in the asynchronous regime, but the calculations become much more complicated and can no longer be made analytically. We must also note that our calculations in the synchronous regime are much simplified because they neglect the backflow effect, necessarily present in this geometry [9]. On the other hand, this effect seems negligible at the centre of the sample where all of our measurements were performed. In the future, it would be interesting to test this hypothesis by numerically solving the complete equations of the nematic dynamics as in the paper of Svenšek and Žumer [16] dealing with backflow effect in nematic LCs confined to a long capillary and subject to a magnetic field.

Acknowledgement

We would like to thank A. Dequidt for his comments and his careful rereading of the article.

Disclosure statement

No potential conflict of interest was reported by the authors.

References

- [1] Fréedericksz V, Repiewa A. Theoretisches und experimentelles zur frage nach der natur der anisotropen flüssigkeiten. *Zeitschrift Für Physik*. 1927;42(7):532–546.
- [2] Tsukada T. TFT/LCD Liquid-crystal displays addressed by thin-film transistors. Amsterdam: Gordon and Breach Publishers; 1996.
- [3] Yeh P, Gu C. Optics of liquid crystal displays. New York: John Wiley & Sons, Inc.; 1999.
- [4] Oswald P, Pieranski P. Nematic and cholesteric liquid crystals: concepts and physical properties illustrated by experiments. Boca Raton (FL): Taylor & Francis, CRC press; 2005.
- [5] De Jeu WH, Claassen WAP. Physical studies of nematic azoxybenzenes. I. Magnetic susceptibilities and the order parameter. *J Chem Phys*. 1978;68:102–108.
- [6] Sherell PL, Crellin DA. Susceptibilities and order parameters of nematic liquid crystals. *J Phys Colloques (Paris)*. 1979;40:C3-211-C3-216.
- [7] Kneppel H, Reiffenrath V, Schneider F. Anisotropy of the magnetic susceptibility of some nematic liquid crystals. *Chem Phys Lett*. 1982;87:59–62.
- [8] Frisken BJ, Carolan P, Palfy-Muhoray P, et al. SQUID susceptibility measurements on 5CB. *Mol Cryst Liq Cryst Lett*. 1986;3:57–62.
- [9] Gasparoux H, Prost J. Détermination directe de l'anisotropie magnétique de cristaux liquides nématiques. *J Phys (Paris)*. 1971;32:953–962.
- [10] Schad HP, Baur G, Meier G. Investigation of the dielectric constants and the diamagnetic anisotropies of cyanobiphenyls (CB), cyanophenylcyclohexanes (PCH), and cyanocyclohexylcyclohexanes (CCH) in the nematic phase. *J Chem Phys*. 1979;71:3174–3181.
- [11] Scheuble BS, Weber G, Eidenschink R. Liquid crystalline cyclohexylcarbonitriles: properties of single compounds and mixtures. *Proc Eurodisplay*. 84-Paris. 1984:65–68.
- [12] Brochard F, Léger C, Meyer RB. Freedericksz transition of a homeotropic nematic liquid crystal in rotating magnetic fields. *J Phys Colloques (Paris)*. 1975;36:C1-209-C1-213.
- [13] Oswald P, Poy G, Vittoz F, et al. Experimental relationship between surface and bulk rotational viscosity in nematic liquid crystals. *Liq Cryst*. 2013;40:734–744.
- [14] Oswald P, Poy G, Dequidt A. Lehmann rotation of twisted bipolar cholesteric droplets: role of Leslie, Akopyan and Zel'dovich thermomechanical coupling terms of nematodynamics. *Liquid Crystals*. 2016;1–20. doi:10.1080/02678292.2016.1255363

- [15] Oswald P. Measurement with a rotating magnetic field of the surface viscosity of a nematic liquid crystal. *Europhys Lett*. 2012;100:26001.
- [16] Svenšek D, Žumer S. Complex backflow dynamics in nematic liquid crystals. *Continuum Mech Thermodyn*. 2002;14:231–239.
- [17] Deuling HJ. Deformation of nematic liquid crystals in an electric field. *Mol Cryst Liq Cryst*. 1972;19:123–131.

Appendix. Exact calculation of the phase diagram without backflow

In this Appendix, we show that Equations (3) and (4) that give the phase lag α and Equations (11) and (12) that define the transition line in the parameter plane (ω, V) remain unchanged in anisotropic elasticity (on condition to take $K = K_3$) when the effects of non-uniformity of the electric field are taken into account.

In our experiment, the frequency of the electric field is much larger than the charge relaxation frequency of the LC, meaning that we are in the dielectric regime. In this regime, the free energy – including the magnetic and electric contributions – reads [17] by assuming from now on that the director field is not twisted ($\partial\varphi/\partial z = 0$):

$$F[\vec{n}, t] = \int_0^d dz \left[\frac{K_3}{2} (1 + \kappa \sin^2\theta) \left(\frac{\partial\theta}{\partial z} \right)^2 - \frac{\chi_a B^2}{2\mu_0} \sin^2\theta \cos^2(\varphi - \omega t) \right] + \frac{1}{2} V D_z \quad (\text{A1})$$

where $V = V(d) - V(0)$ is the applied voltage, $\kappa = \frac{K_1}{K_3} - 1$, $\gamma = -\frac{\varepsilon_a}{\varepsilon_{\parallel}}$ and D_z (constant) is the vertical component of the dielectric displacement vector given by

$$D_z = \frac{-\varepsilon_0 \varepsilon_{\parallel} V}{\int_0^d \frac{dz}{1 + \gamma \sin^2\theta}} \quad (\text{A2})$$

The torque equations follow by writing that

$$\gamma_1 \frac{\partial\varphi}{\partial t} = -\frac{1}{\sin^2\theta} \frac{\delta F}{\delta\varphi} \quad (\text{A3})$$

$$\gamma_1 \frac{\partial\theta}{\partial t} = -\frac{\delta F}{\delta\theta} \quad (\text{A4})$$

which gives

$$\gamma_1 \frac{\partial\varphi}{\partial t} = -\frac{\chi_a B^2}{\mu_0} \cos(\varphi - \omega t) \sin(\varphi - \omega t) \quad (\text{A5})$$

$$\gamma_1 \frac{\partial\theta}{\partial t} = K_3 \frac{\partial^2\theta}{\partial z^2} (1 + \kappa \sin^2\theta) + K_3 \kappa \cos\theta \sin\theta \left(\frac{\partial\theta}{\partial z} \right)^2 + \left[\frac{\chi_a B^2}{\mu_0} \cos^2(\varphi - \omega t) + \frac{D_z^2 \gamma}{\varepsilon_0 \varepsilon_{\parallel} (1 + \gamma \sin^2\theta)^2} \right] \sin\theta \cos\theta \quad (\text{A6})$$

In the stationary regime, we search the solution in the form $\{\varphi(t), \theta(z)\}$ with $\varphi(t) = \omega t - \alpha$. After substitution into Equation (A5), we obtain

$$\alpha = \frac{\pi + \arcsin\left(\frac{\omega}{\omega_*}\right)}{2} \quad (\text{A7})$$

where ω_* is defined in Equation (4). Substitution into Equation (A6) gives after a first integration:

$$\left(\frac{d\theta}{dZ}\right)^2 = \frac{\sin^2\theta_m - \sin^2\theta}{1 + \kappa \sin^2\theta} \left[\frac{(V/V_F)^2}{J^2(1 + \gamma \sin^2\theta)(1 + \gamma \sin^2\theta_m^2)} - (V_B/V_F)^2 \right]. \quad (\text{A8})$$

In this expression, $Z = \pi z/d$, θ_m is the maximum tilt angle at $Z = \pi/2$ to be determined, V_B and V_0 are defined in Equation (8), $V_F = \pi \sqrt{\frac{K_3}{-\varepsilon_0 \varepsilon_a}}$ is the usual critical voltage at zero magnetic field in the bend geometry and

$$J = \frac{1}{\pi} \int_0^\pi \frac{dZ}{1 + \gamma \sin^2\theta} \quad (\text{A9})$$

is an integral to be determined.

From Equation (A8), we obtain after setting $\sin\theta' = \sin\theta_m \sin\psi$:

$$Z = J \int_0^{\arcsin\left(\frac{\sin\theta(Z)}{\sin\theta_m}\right)} d\psi \sqrt{\frac{(1 + \kappa \eta \sin^2\psi)(1 + \gamma \eta \sin^2\psi)(1 + \gamma \eta)}{1 - \eta \sin^2\psi} \left[\left(\frac{V}{V_F}\right)^2 - J^2 \left(\frac{V_B}{V_F}\right)^2 (1 + \gamma \eta \sin^2\psi)(1 + \gamma \eta) \right]}, \quad (\text{A10})$$

where $\eta = \sin^2\theta_m$. This integral equation gives the profile $\theta(Z)$ providing that θ_m and J are known. These two quantities are obtained by expressing that $\theta = \theta_m$ at $Z = \pi/2$ in Equation (A10) and by writing that

$$J = \frac{2}{\pi} \int_0^{\theta_m} d\theta \frac{1}{\frac{d\theta}{dZ}} (1 + \gamma \sin^2\theta). \quad (\text{A11})$$

This procedure gives two equations from which θ_m and J (or D_z , knowing that $D_z = -\frac{\varepsilon_0 \varepsilon_0 V}{dJ}$) can be determined:

$$\frac{\pi}{2} = J \int_0^{\pi/2} d\psi \sqrt{\frac{(1 + \kappa \eta \sin^2\psi)(1 + \gamma \eta \sin^2\psi)(1 + \gamma \eta)}{1 - \eta \sin^2\psi} \left[\left(\frac{V}{V_F}\right)^2 - J^2 \left(\frac{V_B}{V_F}\right)^2 (1 + \gamma \eta \sin^2\psi)(1 + \gamma \eta) \right]}, \quad (\text{A12})$$

$$\frac{\pi}{2} = \int_0^{\pi/2} d\psi \sqrt{\frac{(1 + \kappa \eta \sin^2\psi)(1 + \gamma \eta)}{(1 - \eta \sin^2\psi)(1 + \gamma \eta \sin^2\psi)} \left[\left(\frac{V}{V_F}\right)^2 - J^2 \left(\frac{V_B}{V_F}\right)^2 (1 + \gamma \eta \sin^2\psi)(1 + \gamma \eta) \right]}. \quad (\text{A13})$$

At the onset of instability, the two previous equations have a trivial analytical solution corresponding to $\theta = 0, \forall Z$. As a consequence $\eta = 0, J = 1$ and $\frac{V^2 - V_B^2}{V_F^2} = 1$ at the onset of instability. This last equation is the same as Equation (11) given in Section 2 on condition to replace K by K_3 . The main interest of this calculation is to show that the tilt angle profile can be exactly calculated by solving numerically Equations (A10), (A12) and (A13) (under the assumption that the backflow is negligible).